Basic Neuroscience

# Monitoring synaptic and neuronal activity in 3D with synthetic and genetic indicators using a compact acousto-optic lens two-photon microscope☆

Tomás Fernández-Alfonso, K.M. Naga Srinivas Nadella, M. Florencia Iacaruso, Bruno Pichler, Hana Roš, Paul A. Kirkby, R. Angus Silver *

*Department of Neuroscience, Physiology and Pharmacology, University College London, London WC1E 6BT, UK*

## HIGHLIGHTS

- We expand the utility of acousto-optic lens (AOL) 3D 2P microscopy.
- We show rapid, simultaneous monitoring of synaptic inputs distributed in 3D.
- First use of genetically encoded indicators with AOL 3D functional imaging.
- Measurement of sensory-evoked neuronal population activity in 3D *in vivo*.
- Strategies for improving the measurement of the timing of neuronal signals.

## GRAPHICAL ABSTRACT
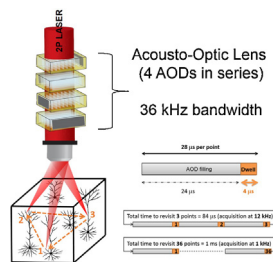


## ARTICLE INFO

## ABSTRACT

*Background:* Two-photon microscopy is widely used to study brain function, but conventional microscopes are too slow to capture the timing of neuronal signalling and imaging is restricted to one plane. Recent development of acousto-optic-deflector-based random access functional imaging has improved the temporal resolution, but the utility of these technologies for mapping 3D synaptic activity patterns and their performance at the excitation wavelengths required to image genetically encoded indicators have not been investigated.

*New method:* Here, we have used a compact acousto-optic lens (AOL) two-photon microscope to make high speed [$Ca^{2+}$] measurements from spines and dendrites distributed in 3D with different excitation wavelengths (800–920 nm).

*Results:* We show simultaneous monitoring of activity from many synaptic inputs distributed over the 3D arborisation of a neuronal dendrite using both synthetic as well as genetically encoded indicators. We confirm the utility of AOL-based imaging for fast *in vivo* recordings by measuring, simultaneously, visually evoked responses in 100 neurons distributed over a 150 μm focal depth range. Moreover, we explore ways to improve the measurement of timing of neuronal activation by choosing specific regions within the cell soma.

*Comparison with existing methods:* These results establish that AOL-based 3D random access two-photon microscopy has a wider range of neuroscience applications than previously shown.

*Conclusions:* Our findings show that the compact AOL microscope design has the speed, spatial resolution, sensitivity and wavelength flexibility to measure 3D patterns of synaptic and neuronal activity on individual trials.

## 1. Introduction

Understanding how the brain represents and processes information in the form of electrical and chemical signals is a central aim of neuroscience. Neuronal signals are typically brief (1–100 ms) and are sparsely distributed in 3D space: in the patterns of activated synapses on the dendritic tree of an individual neuron and in the electrical activity of populations of neurons within a network. Recent work shows that representation and processing of sensory information by networks can occur on very fast time scales (1–100 ms) (Gollisch and Meister, 2008; Harvey et al., 2013; Johansson and Birznieks, 2004; Junek et al., 2010). Signalling on this time scale is also important for both synaptic integration and synaptic plasticity (Sjostrom et al., 2008). Assaying the computational state of a neuron or a network of neurons therefore requires a device that can monitor activity at many different locations in 3D space at high temporal and spatial resolution.

Two-photon microscopy (Denk et al., 1990) enables neural activity to be monitored with high spatial resolution deep within scattering tissue (Helmchen and Denk, 2005; Zipfel et al., 2003). This allows $[Ca^{2+}]$ to be monitored in spines and dendrites (Chalifoux and Carter, 2011; Higley and Sabatini, 2012; Noguchi et al., 2005; Svoboda et al., 1999) and receptive fields to be mapped at both the cellular (Kerr et al., 2005, 2007; Ohki et al., 2005; Sato et al., 2007) and subcellular (Bollmann and Engert, 2009; Jia et al., 2010) level. However, conventional galvanometer-based whole-frame imaging is ~30–100-fold too slow, and multiline imaging (Bonifazi et al., 2009) and custom line scans (Rothschild et al., 2010) are 10-fold too slow to identify spike timing in neuronal populations on the millisecond timescale. In addition, functional measurements are restricted to a single plane, a major constraint since neurons and networks are inherently 3D structures.

Several new innovations have enabled more rapid 2-photon imaging in 2D and 3D (Botcherby et al., 2012; Katona et al., 2011; Kirkby et al., 2010; Nikolenko et al., 2008; Vucinic and Sejnowski, 2007). The fastest of these uses acousto-optic deflectors (AODs) to point in 2D (Grewe et al., 2010; Salome et al., 2006), raster scan in 2D (Chen et al., 2011; Kirkby et al., 2010) or to make 3D Random Access MultiPhoton (RAMP) point measurements (Duemani Reddy et al., 2008; Katona et al., 2012; Kirkby et al., 2010). However, AOD-based 3D-RAMP imaging has been limited by inefficient light transmission, temporal dispersion, limited spatial resolution and fixed wavelength excitation. These side effects of using AODs potentially limit the study of distributed signalling in small structures, such as spines, and prevent the use of this technology with genetically encoded indicators, which are typically excited at longer wavelengths than their synthetic counterparts (*e.g.*, GCaMP3 at ~900 nm *vs* Fluo-4 at ~800 nm). Here, we describe the performance of a recently developed 2-photon microscope that uses 4 custom-designed optically and acoustically rotated AODs to form a compact AOL that can be fitted to a conventional 2-photon microscope allowing 3D-RAMP at 36 kHz bandwidth (Kirkby et al., 2010). We tested its utility for high-speed 3D functional imaging of neuronal activity using $[Ca^{2+}]$ indicators, both *in vitro* and *in vivo*. We demonstrate two advances over previous 3D-RAMP measurements with AOL microscopes (Duemani Reddy et al., 2008; Katona et al., 2012). First, we show that our AOL microscope can be used to simultaneously monitor many synaptic inputs onto dendritic spines distributed over 3D dendritic trees on single trials. Secondly, we show that AOL microscopes can operate at the long laser wavelengths required for imaging genetically encoded indicators.

## 2. Methods

All experimental procedures were carried out in accordance with institutional animal welfare guidelines and licensed by the UK Home Office.

### 2.1. In vitro experiments

#### 2.1.1. Slice preparation

C57BL/6 (or CD1, see below) mice (P14–22) were anaesthetized with isoflurane, sacrificed and their brains removed. Slices of the somatosensory cortex were cut in ice-cold solution (in mM): 85 NaCl, 2.5 KCl, 24 NaHCO$_3$, 1.25 NaH$_2$PO$_4$, 0.5 CaCl$_2$, 4 MgCl$_2$, 25 glucose, 75 sucrose, bubbled with 95% O$_2$/5% CO$_2$. Slices were cut 350 μm thick in either the parasagital (Agmon and Connors, 1991) or coronal orientation and incubated in artificial cerebrospinal fluid (ACSF; in mM: 125 NaCl, 2.5 KCl, 26 NaHCO$_3$, 1.25 NaH$_2$PO$_4$, 2 CaCl$_2$, 1 MgCl$_2$, 25 glucose and 0.5 ascorbic acid, bubbled with 95% O$_2$/5% CO$_2$) at 30–35 °C for 30–45 min, and then kept at room temperature for up to ~6 h before experiments were carried out in ACSF at ~30 °C.

#### 2.1.2. Electrophysiology

Patch pipettes (3–6 MΩ) were filled with internal solution containing (in mM): 130 KMeSO$_3$; 10 Na-Phosphocreatine; 10 Hepes; 4 MgCl$_2$; 4 Mg$_2$-ATP; 0.3 Na$_2$-GTP; 0.5 EGTA. An alternative solution replacing KMeSO$_3$ with K-gluconate (125 mM), without EGTA, was also used in some experiments. Alexa 594 and Fluo-4 (invitrogen) were added to the internal solution at 20–200 μM and 100–200 μM, respectively. Current-clamp recordings began ~20 min after establishing whole-cell access (series resistance < 30 MΩ) to allow dye diffusion into dendrites. Recordings were made *via* an Axoclamp 200B amplifier (Molecular Devices), low-pass filtered at 10 kHz, and acquired at 50 kHz sampling rate using Neuromatic (http://www.neuromatic.thinkrandom.com/) running within the IgorPro environment (Wavemetrics).

#### 2.1.3. In utero electroporation

Electroporation of GCaMP3 (plasmid #22692, Addgene) was carried out in CD1 mice. DNA was prepared using the EndoFree Plasmid Maxi Kit (Qiagen, Hilden, Germany) and diluted from 4 μg/μl to 1–2 μg/μl in Tris–EDTA buffer (Sigma) with Fast Green (Sigma) prior to surgery. *In utero* electroporation was carried out at E16.5 (the morning of a detectable vaginal plug and the first neonatal day were considered to be embryonic day 0.5 and postnatal day 0, respectively) to express DNA specifically in pyramidal neurons of L2/3 of one cortical hemisphere, as described previously (Saito and Nakatsuji, 2001; Tabata and Nakajima, 2001) with slight modifications. Briefly, pregnant mice were deeply anesthetized with ketamine (80 mg/kg i.p.), xylazine (10 mg/kg i.p.) and buprenorphine (0.05–0.1 mg/kg s.c.), supplemented when necessary until the animal was unresponsive to foot/tail pinch stimuli, while the body temperature was maintained at 37 °C using a feedback temperature controller and the uterine horns were exposed. Glass

pipettes (tip diameter ~50 μM; 1.5 mm glass; World Precision Instruments) were pulled on a P-97 horizontal puller (Sutter Instruments) and filled with DNA solution. 1–2 μL of DNA solution was pressure injected (Picospritzer, General Valve) into the right lateral ventricle of the embryo. The head of the embryo was placed between tweezer electrodes with the positive plate contacting the right side of the head. Electroporation was achieved with five square pulses (duration 50 ms, frequency 1 Hz, 37 V) using an electroporator (ECM830, BTX). Care was taken to quickly place embryos back into the abdominal cavity to avoid temperature loss. The wall and skin of the abdominal cavity were sutured, and embryos were allowed to develop normally. The transfected cortical region in electroporated animals was always restricted to L2/3 in the electroporated hemisphere. It usually encompassed most of the barrel cortex and in some cases included parts of auditory, visual and secondary somatosensory areas.

### 2.2. In vivo experiments

#### 2.2.1. Surgery and dye injection

C57BL/6 mice (P25-P33) were anaesthetized with a mixture of Fentanyl (0.05 g/kg), Midazolam (5.0 mg/kg) and Medetomidin (0.5 mg/kg) for surgery and recordings. Surgery was performed as described previously (Ko et al., 2011). Briefly, a small craniotomy (1–2 mm) was carried out over primary visual cortex and sealed after dye injection with 1.6% agarose in HEPES-buffered ACSF and a cover slip. Fluo-4AM and Calcein red-orange-AM (Molecular Probes) were initially dissolved to 5 mM with 20% Pluronic Acid in DMSO (Pluronic F-127, Molecular Probes) and further diluted with dye buffer (150 mM NaCl, 2.5 mM KCl, and 10 mM HEPES, pH 7.4) to a final concentration of 250 μM and 25 μM, respectively, in the same solution. Oregon-Green Bapta 1-AM (OGB1-AM) was first dissolved to 10 mM and further diluted to a final concentration of 0.9 mM before injection. Dyes were slowly pressure-injected into the right visual cortex at a depth of 150–200 μm with a micropipette (3–5 MΩ, 3–10 p.s.i., 2–4 min) under visual control by 2-photon imaging (10× water immersion objective, Olympus). Experiments started 1–2 h after dye loading. A total of 3 in vivo experiments are presented, one with OGB1-AM (Fig. S3) and two with Fluo4-AM (Fig. 6 and S5).

#### 2.2.2. Visual stimulation

Visual stimuli were generated using MATLAB Psychophysics Toolbox (Brainard, 1997; Pelli, 1997), and displayed on an LCD monitor (375 mm × 300 mm; 60 Hz refresh rate) positioned 20 cm from the left eye, at approximately 45 degrees to the long axis of the animal, covering ~86 × 74 degrees of visual space. A stimulation sequence comprised the presentation of gratings (i.e., consecutive black and white stripes, 0.04 cycles per degree) in 8 different orientations (45° steps). Fluorescence acquisition during each orientation lasted 2 s, starting with a motionless grating that began to drift at a constant rate (2 cycles per second; normal to the stripes length) after 400 ms and for the remaining time. The display was then shifted to the next orientation before the next 2-s trial started.

### 2.3. AOL-based two-photon imaging

#### 2.3.1. Microscope layout

The AOL microscope consisted of a tunable femtosecond laser source, a customized prechirper to compensate for the temporal dispersion introduced by the AOL, and a compact AOL (Kirkby et al., 2010), together with the relay optics required to route the beam into a conventional two-photon microscope (Fig. 1A). The specific components were as follows (from light source to sample): a laser (Mai Tai, Newport-Spectra Physics or Chameleon Ultra II, Coherent), a custom prechirper (−50,000 fs$^2$ GVD, APE GmbH,
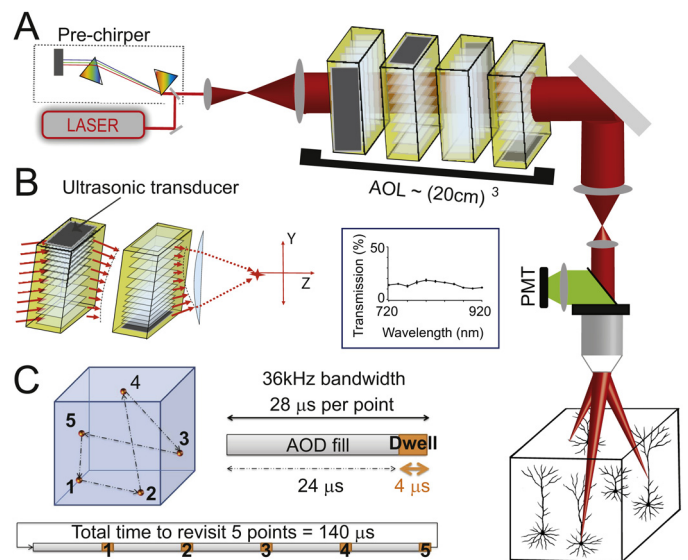


**Fig. 1.** A compact acousto-optic lens (AOL) microscope for two-photon functional imaging in 3D at 36 kHz bandwidth.

(A) Main optical components of the AOL microscope: a femtosecond laser source, a customized prechirper to compensate for temporal dispersion, a beam expander, 4 custom-designed acousto-optic deflector (AOD) crystals in series, together with a conventional 2-photon microscope including photomultiplier tube (PMT) detection. Cartoon below showing focusing and steering of a laser beam to 3 points of interest (POI) within neural tissue. Inset AOL efficiency (fraction of laser power transmitted through the AOL) during operation of the laser at wavelengths used in neuroscience applications. (B) Illustration of remote focusing of laser beam with two AODs. Linearly varying sound waves created by ultrasonic transducers (grey sheets) transformed the planar optical wavefront into a curved wavefront, thereby focusing the beam in the Z axis. A counter-propagating acoustic wave in the second crystal transiently compensates for movements in the X axis, enabling the laser beam to be transiently focused in the XZ plane. (C) Cartoon illustrating random access measurements from 5 POIs. It takes 28 μs to revisit each point (24 μs for a sound wave to fill the AOD plus 4 μs dwell time), giving a total serial bandwidth of 36 kHz, which divided across 5 selected POIs is 7 kHz.

Berlin), a Pockels cell (Conoptics Model 302CE), a beam expander, the AOL, relay optics (including an Ultima scanhead, Prairie Technologies), an upright microscope (BX51, Olympus) with tube lens and IR antireflection coated water-immersion objective (Olympus LumPLanFL/IR 40x/0.80W or 20x/0.95W), and conventional photon collection and detection components (see below).

#### 2.3.2. The acousto-optic lens

##### 2.3.2.1. Design and general operation.

The AOL was constructed of 4 acousto-optic deflector (AOD) crystals, half waveplates (ACWP-700-1000-10-2, CVI Laser Optics) and linear polarizers (ColorPol VIS 700 BC4 CW02, CODIXX AG, Germany) arranged in series. The custom-designed AOD crystals were optically and acoustically rotated and the second crystal of each pair had narrower ultrasonic transducers (Kirkby et al., 2010). They were manufactured by Gooch & Housego (Somerset, UK) following our specifications (Supplementary Table 2). High speed remote focusing to different locations within the 3D field of view was achieved by driving each AOD with ultrasonic sound waves (range 25–47 MHz), which produced a diffraction grating across the crystal (Fig. 1B). The focus (Z direction) was altered by changing the slope of the linear frequency ramp of the acoustic drive (chirping), while lateral displacement was achieved by offsetting the ramp frequencies. Two AODs, with counter propagating sound waves, were used to cancel out the movement introduced by the sound propagating across the crystals allowing a stationary focus (Kaplan et al., 2001). Each pair of crystals formed a cylindrical lens that focused and steered the beam along the X–Z and Y–Z planes, with the two orthogonally aligned pairs forming a dynamic spherical lens (i.e., the AOL) in a
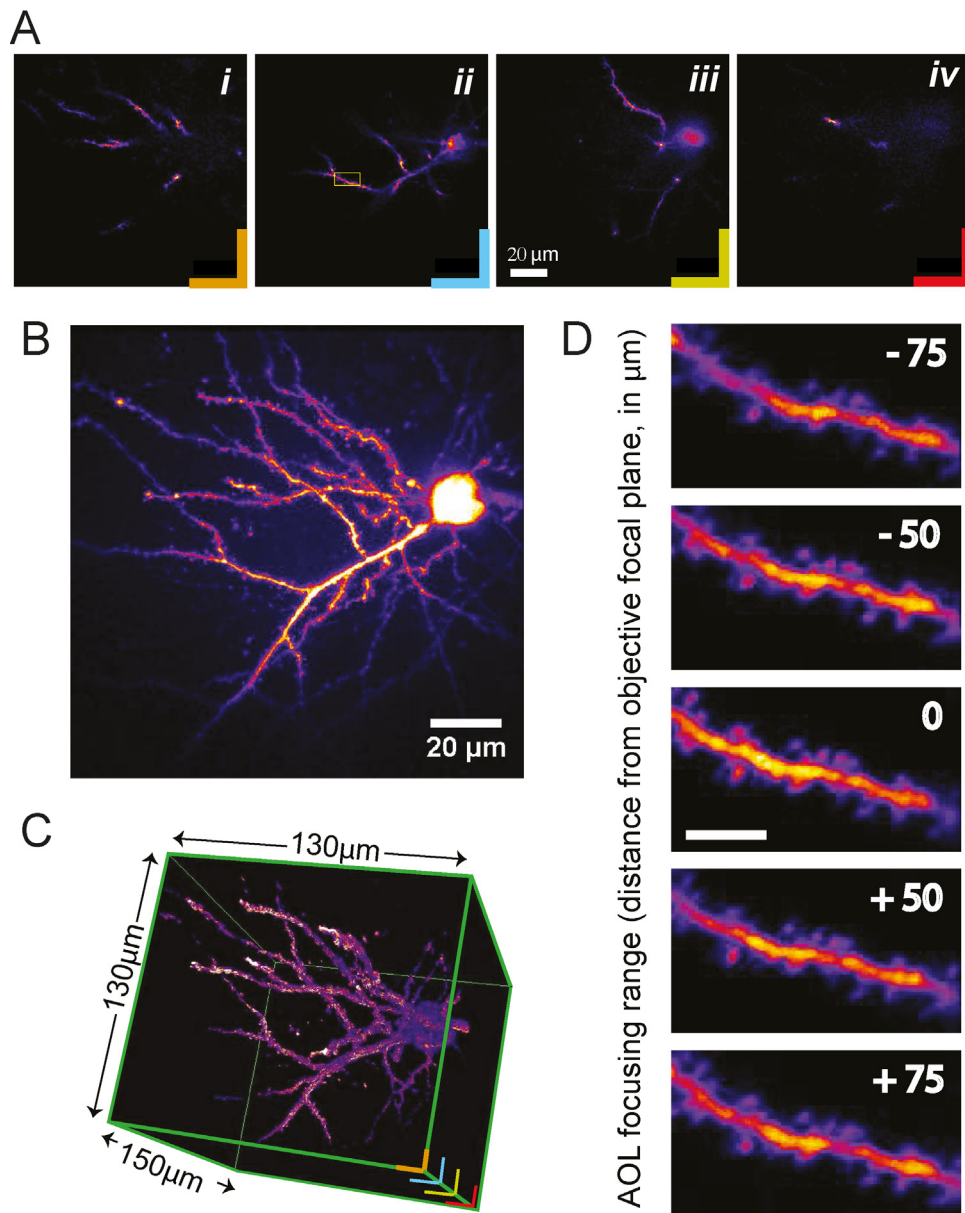
**Fig. 2.** AOL-based volumetric structural imaging of neuronal dendrites and spines over a 150 μm depth range.
(A) Examples of 2D images of a pyramidal cell patch-loaded with the fluorescent dye Alexa 594 (200 μM) and focused with the AOL at different depths from top of slice (15 μm, 45 μm, 90 μm and 145 μm for i, ii, iii and iv, respectively). (B) Maximum intensity projection (MIP) constructed from the Z-stack of structural images encompassing a 150 μm range in depth (100 focal planes spaced every 1.5 μm). (C) 3D rendering of the same images as B. (D) AOL-based images of the same dendritic section at different focal depths with respect to the natural focal plane of the objective. The defocus introduced by physical Z displacement of the objective between −75 μm and +75 μm was compensated for by the AOL (display gain was enhanced at +75 μm and −75 μm, see Materials and methods).

compact configuration without telecentric relays between the AODs (Kirkby et al., 2010). The AOL could address, sequentially, any voxel within the volumetric field of view in 24 μs regardless of the distance between points (Fig. 1C) (Kirkby et al., 2010). Combining this with a dwell time of 4 μs gave a total acquisition time per point of 28 μs or a total serial bandwidth of 36 kHz. The compact design of the AOL simplified its physical introduction into an existing two-photon system, since it occupied only ∼20 cm of the input beam path (Fig. 1A). The maximal power achieved at the back aperture of the objective was 150 mW (800 nm) which was sufficient for deep *in vivo* imaging given the narrow pulse width (110–160 fs). Typical imaging powers in were 5–20 mW and 20–80 mW at the back aperture for *in vitro* and *in vivo* experiments, respectively.

*2.3.2.2. Operation at 720–920 nm wavelengths and power throughput.* During imaging at 800 nm, the acoustic centre frequency was set at 35 MHz. Since the angle of diffraction produced by the acoustic wave filling the AOD crystal depends on the optical wavelength of the incoming laser beam (*i.e.*, $\emptyset = \lambda\, f/V_{ac}$, where $\emptyset$ is the angle of diffraction, $\lambda$ is the wavelength of the optical beam, $f$ is acoustic wave frequency driven by the ultrasonic transducer and $V_{ac}$ is the acoustic velocity through the crystal, see Kirkby et al., 2010), changes in imaging wavelength ($\lambda$) were compensated for by changing the acoustic centre frequency ($f_c$) of the crystals, thereby keeping the diffraction angle constant (*i.e.*, $f_{c2} = \lambda_2\, f_{c1}/\lambda_1$). Thus, when the excitation wavelength was set at 800 nm, 870 nm or 920 nm, the acoustic centre frequency was 35 MHz, 32.2 MHz or 30.4 MHz, respectively. While mechanically the AOL was unaltered, wavelength changes involved tuning the motorized prisms and the mirror within the prechirper. Measurements of power throughput across the AOL showed that the efficiency of light transmission was 10-18% at wavelengths
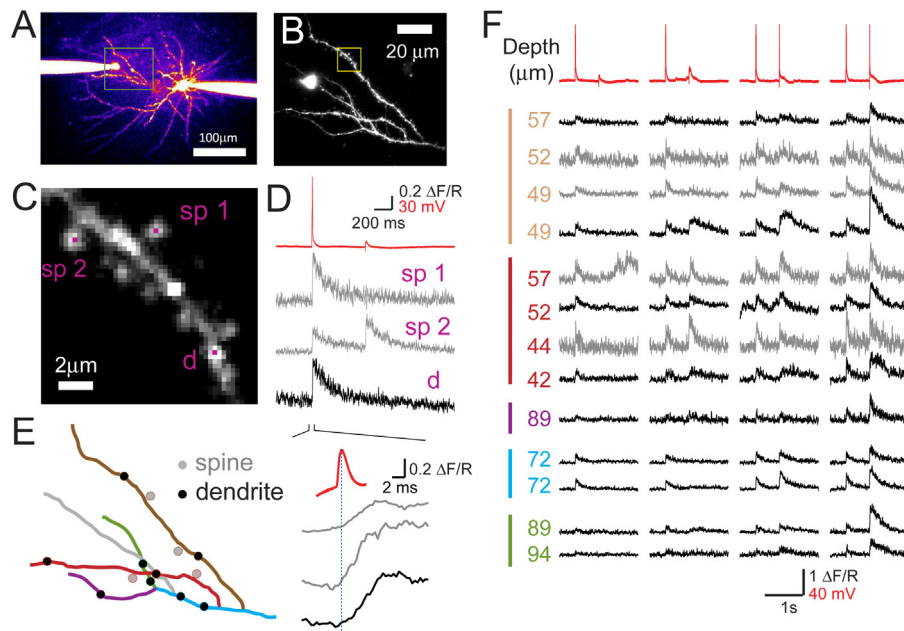
**Fig. 3.** 3D functional imaging of synaptic inputs on spines and dendrites using a synthetic calcium indicator.
(A) MIP of a L2/3 cortical neuron patch loaded with a green calcium indicator (Fluo-4) and a red morphological tracer dye (Alexa 594) imaged with the AOL microscope at 800 nm wavelength. A second pipette for synaptic stimulation is shown on the left. (B) MIP of region of dendritic tree spanning 70 μm in depth selected for functional imaging (box in A). (C) A dendritic branch (box in B) with 3 selected POI on spines (Sp1 & 2) and shaft (d) (1 pixel = 260 nm). (D) Single-trial [Ca2+] measurements (ΔF/R) during an AP, evoked by injecting current through the somatic electrode, followed by extracellular synaptic stimulation (2.4 kHz acquisition filtered with 4 ms window). Whole-cell voltage recordings in red. (E) Schematic diagram of dendritic branches in B showing the POIs selected in the volumetric field of view for functional imaging (spines in grey and shaft in black). (F) Increasing synaptic stimulation intensity from left to right columns (1.2 kHz acquisition filtered with 8 ms window). Within each branch (colour coded line on the right) single-trial traces are arranged from most proximal at the top to [Ca2+] measurements at POIs during neuronal activation as in D. Four consecutive trials with increasing stimulation intensity, with most distal from soma at the bottom. The POI depth from top of the slice is shown on the left.

typically used in neuroscience applications (720–920 nm) (inset of Fig. 1A).

### 2.3.3. Collection of photons and data acquisition

Emitted photons, collected through the objective, were separated from excitation photons using a 660 nm long-pass dichroic mirror (660dcxr) followed by a 650 nm short-pass filter. Green and Red emitted photons were further isolated using a 575 nm long-pass dichroic (575dcxr) and emission filters (HQ 525/70-2P and HQ 630/100-2P, respectively), and detected using GaAsP (Hamamatsu H7422) and multialkali (Hamamatsu R3896) photomultipliers (PMTs), respectively. During *in vitro* experiments, an extra set of dichroics, filters and PMTs were used to detect fluorescence photons collected through an achromatic aplanar condenser (Olympus U-AAC, 1.4 NA) underneath the stage. Filters and dichroics were from Chroma Technology. PMT signals were amplified and low-pass filtered at 1.25 MHz (Prairie Technologies), digitized (12bit) at 1 MHz (National Instruments PCI-6115) and down-sampled at 250 kHz (average of 4 consecutive digitizations) during acquisition with custom-made software written in Labview (National Instruments). At each point, a single 4 μs dwell time (see Fig. 1C) was used for both structural imaging and 3D RAMP measurements. Excitation light was shuttered with a Pockels cell except during 4–12 μs spanning the 4 μs dwell time. Laser intensity was modulated exponentially with depth using the Pockels cell in order to compensate for scattering (Chaigneau et al., 2011). Although the AOL microscope can be used to do ultra-rapid raster scanning (Kirkby et al., 2010), in this work structural imaging was carried following sequential pointing and images reconstructed from "red" or "green" channel (for experiments with synthetic or genetic indicators respectively). Except for the images shown in Fig. S1 A–B, which were taken with an underfilled 20× objective (Olympus) which gave a field of view (FOV) of

250 μm × 250 μm × 150 μm, all functional and structural imaging was done with a 40×, 0.8NA objective. Single focal plane images were typically 130 μm × 130 μm (cropped to 80–130 μm per axis to display) except in Fig. 2D which was zoomed 8 times. Images were reconstructed with 512 × 512 pixels (Figs. 2–5) or 200 × 200 pixels (rest of figures). The display in Fig. 2D was shown with different gain display settings for −75 μm and +75 μm to compensate for a slight drop in excitation efficiency, which is likely to be due to optical aberrations (Kirkby et al., 2010).

### 2.4. Data analysis

Structural images were displayed and rendered using ImageJ. Data was analyzed using Neuromatic and custom-written routines in IgorPro6 (Wavemetrics). Changes in Fluo-4 fluorescence were expressed relative to its baseline fluorescence (ΔF/F) or to the average fluorescence of the red morphological tracer (ΔF/R). Changes in GCaMP3 fluorescence were expressed as ΔF/F. The average of a sliding boxcar smoothing window (length reported in Fig. legends) was used to digitally filter the data. Data are presented as mean ± standard deviation (SD) unless otherwise stated. Signal to Noise Ratio (SNR) was calculated as the peak of the fit to the [Ca2+] transient divided by the standard deviation of the baseline signal calculated over 200–400 ms. Fluorescence transients were fit to a tri-exponential function with two decay components (Nielsen et al., 2004):

$$F(t) = \left(1 - e^{-(t-t0)/\tau r}\right)^N \times \left(A_1 e^{-(t-t0)/\tau 1} + A_2 e^{-(t-t0)/\tau 2}\right),$$

where the exponent $N$ produces a small "foot" at the beginning of the transient ($N$ between 1 and 4). The rise time reported refers to the time taken for the fit of the signal to rise from 10% to 90% of the peak value. The decay corresponds to the time for the fitted function (equation above) to decay to 37% of its peak value. Fluorescence
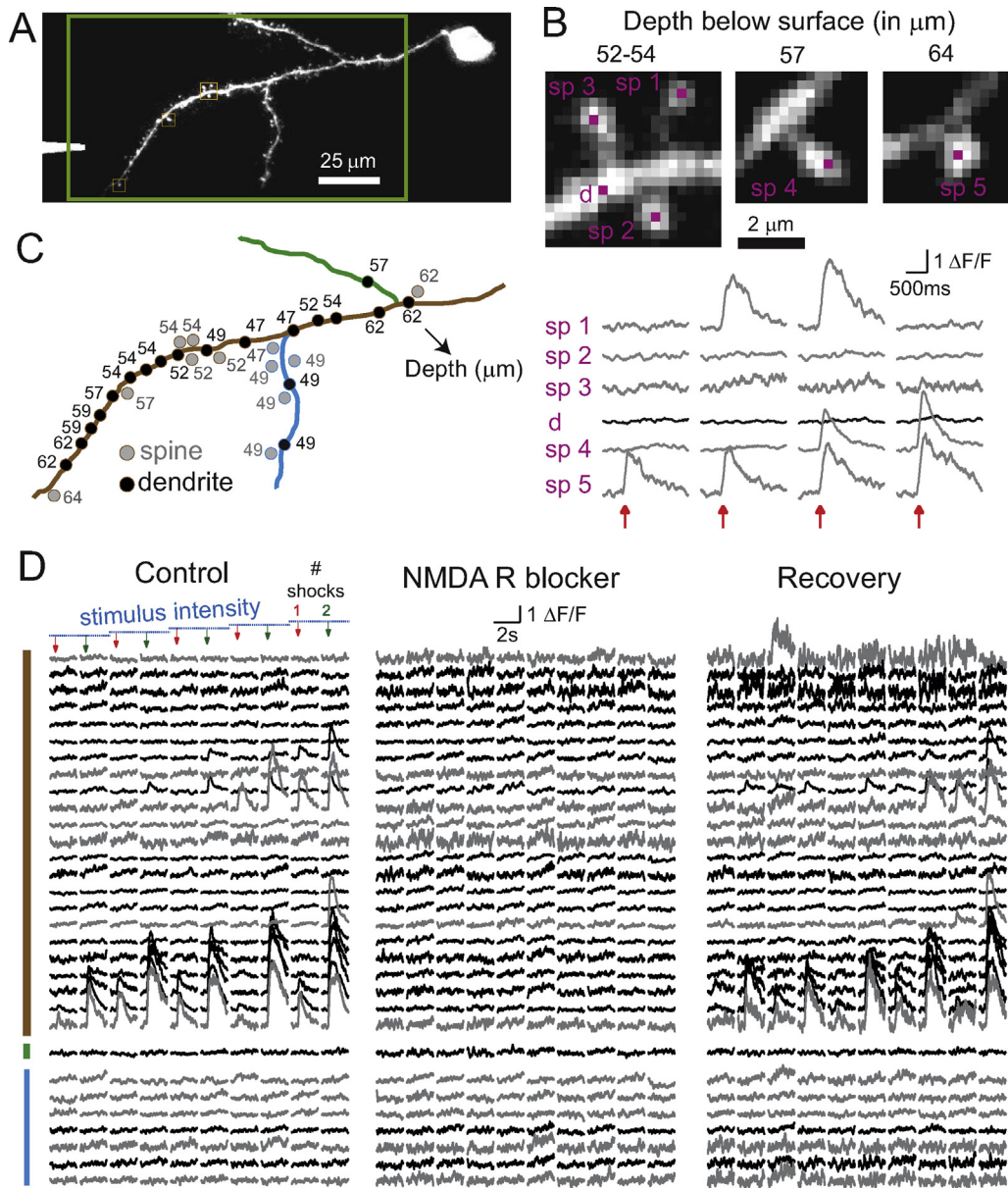
**Fig. 4.** 3D functional imaging of synaptic inputs on spines and dendrites using a genetically encoded calcium indicator.
(A) Background-excluded MIP 40–64 μm below slice surface) of a L2/3 pyramidal cell expressing GCaMP3 imaged at 870 nm wavelength. Extracellular synaptic stimulation pipette (at 50 μm depth) is visible on the left. (B) Montage of single plane images of spines at different dendritic locations and depths. Traces below show simultaneous single-trial GCaMP3 based [Ca²⁺] measurements from 5 spines and dendrite locations in images for 4 trials with increasing extracellular stimulation intensity (arrow, single stimulus). (C) Schematic of dendrites and spines showing 31 POIs selected for functional measurements. Numbers indicate depth in μm, of POI from top of the slice. (D) Simultaneous measurements of GCaMP3 fluorescence changes in the 31 locations shown in C. POIs are arranged from proximal to distal (top to bottom, spines in grey and dendrites in black) in each branch (colour coded rightmost line). Each column is a single trial lasting 2 s. Stimulation voltage was increased every pair of trials consisting of a single and double shock (red and green arrows, respectively). Middle and right block show same protocol in presence of 10 μM APV and following washout, respectively. Data was acquired at 0.9 kHz/POI and filtered with a 100 ms window. (For interpretation of the references to color in this figure legend, the reader is referred to the web version of this article.)

amplitudes were calculated from the fitted function. The 95% confidence interval for the estimated action potential (AP) time was calculated from 4 times the S.D. of the onset times (the time at which the signal rose to 10% of its peak value) of the fluorescent transients.

## 3. Results

### 3.1. Spatial resolution of the AOL microscope

To test the performance of the AOL microscope for resolving small biological structures in brain tissue, we imaged layer 2/3 (L2/3) pyramidal cells loaded with the red synthetic tracer dye Alexa 594 in acute slices of mouse neocortex. The field of view with a fully back-filled 40 × 0.8NA water immersion objective was 130 μm × 130 μm in the X–Y plane and extended over a 150 μm depth (Fig. 2A–C), and represents the maximum volume that can be imaged simultaneously with high temporal and spatial resolution. The maximum intensity projection (MIP) (Fig. 2B) and 3D projection (Fig. 2C) of 100 planes show a large part of the dendritic tree of a L2/3 pyramidal neuron within the imaging volume. A side-by-side comparison of Z stacks acquired by AOL focusing, when the microscope objective was fixed, vs conventional focusing with objective displacement gave a similar imaging quality for the same
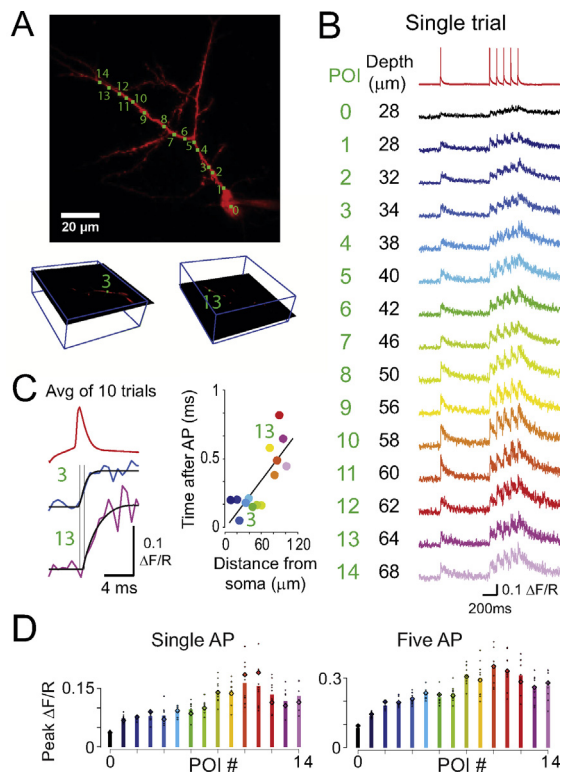
**Fig. 5.** High speed functional imaging of [Ca$^{2+}$] transients evoked by an action potential as it backpropagates into a 3D dendritic tree.
(A) MIP of L2/3 pyramidal cell patch-loaded with Fluo-4 (100 μM) and Alexa 594 (20 μM) showing 15 POIs selected for functional imaging. Two representative planes at different depths shown below. (B) Single trial [Ca$^{2+}$] signals during a single AP followed by a burst of 5 evoked APs (red trace on top) recorded simultaneously at 1.6 kHz from 15 POIs, with their respective depth from top of slice indicated on left. (C) Examples of averaged [Ca$^{2+}$] transients on a fast timescale (POIs 3 and 13, fit to transient shown in black). Right, relationship between onset of AP-evoked [Ca$^{2+}$] transient and distance of measurement locations from soma. The slope of the linear fit of tri-exponential function was 0.17 m/s. (Spearman correlation coefficient = 0.73, $R = 0.81$, $p = 0.00022$). (D) Peak amplitude ($\Delta F/R$) of AP-evoked [Ca$^{2+}$] transients in response to a single (left) or 5 APs (right). Each trial is represented with a circle and the bar height is the average of 10 trials. The coloured bins correspond to the trials shown in B. (For interpretation of the references to color in this figure legend, the reader is referred to the web version of this article.)

volume (Suppl. Movie 1). Moreover, using the AOL to compensate for the focus when the objective was physically displaced, so that the focal plane of the objective was above or below the imaged dendrite, shows that submicrometer spines can be resolved over the entire 150 μm focusing range of the AOL using a modest amount of power (10–15 mW at the back aperture) (Fig. 2D), consistent with the point spread function (PSF) dimensions over this focal range (0.35–0.7 μm; Supplementary Table 1 and Fig. 16 of Kirkby et al., 2010).

### 3.2. Simultaneous monitoring of spatially distributed synaptic inputs in 3D

#### 3.2.1. Functional imaging of dendrites and spines with a synthetic [Ca$^{2+}$] indicator

To test the functional performance of the AOL microscope, we whole-cell patch clamped the soma of L2/3 pyramidal cells and loaded them with two synthetic dyes: the Ca$^{2+}$ indicator Fluo-4 (green) and Alexa 594 (red) to visualize the neuron (Fig. 3A). A region of the dendritic tree was identified and a second pipette was placed near one of the dendritic branches for local extracellular synaptic stimulation (Fig. 3A and B). Fig. 3C shows a short section of dendrite, with two points of interest (POI) in neighbouring

spines and a third in the shaft. Triggering a single action potential (AP) with current injection through the somatic electrode produced large, rapidly rising and decaying [Ca$^{2+}$] transients simultaneously at all three dendritic locations (Fig. 3D). In contrast, local extracellular stimulation of synaptic input only triggered a [Ca$^{2+}$] transient in spine 2, with no detectable [Ca$^{2+}$] transient in spine 1, just 5 μm away, consistent with previous observations (Bloodgood and Sabatini, 2007; Chalifoux and Carter, 2011; Noguchi et al., 2005). These results show that the spatial resolution of the AOL microscope and signal-to-noise ratio (SNR) of functional measurements are sufficiently high to enable us to distinguish synaptic activation from failures in individual spines on a single trial. Next, to investigate how backpropagating APs and synaptic input affected dendritic [Ca$^{2+}$] on a larger scale, we examined the responses in spines and dendrites distributed in 3D across a substantial part of the dendritic tree (Fig. 3E). Simultaneous recordings from 13 POIs located between 42 μm and 94 μm from the surface of the slice revealed that all locations responded to the somatically evoked AP, but that weak synaptic stimulation only produced a response in a subset of locations (Fig. 3F, left pair of columns). Increasing the strength of synaptic stimulation to a level that triggered an AP produced a widespread [Ca$^{2+}$] transient (Fig. 3F, last two columns). These results show that the AOL microscope has the spatial and temporal resolution to simultaneously monitor the activity of spines distributed in 3D across multiple dendritic branches.

#### 3.2.2. Functional imaging of dendrites and spines with a genetically encoded [Ca$^{2+}$] indicator

Genetically encoded indicators have two main advantages over synthetic indicators: they can be used to target specific cell populations and they can be expressed for prolonged periods, enabling both cell-type specific and chronic functional measurements. To assess the performance of our AOL microscope with genetically encoded [Ca$^{2+}$] indicators we expressed GCaMP3 in L2/3 pyramidal cells by performing *in utero* electroporation of a plasmid encoding GCaMP3 (Tian et al., 2009). To image at the longer excitation wavelengths required, we changed the acoustic centre frequency of the AOL drive, without having to physically adjust any of the AOL optical elements. Images of acute slices of sensory cortex taken at low magnification during excitation at 870–920 nm revealed the presence of GCaMP3 in a subset of L2/3 neurons (Fig. S1 A and B). At higher magnification, dendrites and spines were evident (Fig. S1C). Functional measurements from dendrites spanning a 90 μm depth revealed the presence of a dendritic section that responded to both single and bursts of electrical stimuli (Fig. S1 C and D). Fig. 4A shows a MIP image in which a mask outlining a subset of in-focus dendritic segments was used to isolate the dendrites of interest in multiple planes (Movie S2 shows the unedited version of each plane). To study the recruitment of synapses and the [Ca$^{2+}$] profile along the dendrite we placed POIs on spines and shafts of the distal dendritic tree, 47–64 μm below the surface of the slice, and made 3D-RAMP measurements at different stimulation intensities (Fig. 4B and C). Fig. 4B, which shows three examples of spines at different dendritic locations, shows that the stimulus-evoked GCaMP3 signals were localized to particular spines, while others nearby did not respond. While minimal intensity stimulation recruited few spines across the dendrite, more were recruited as the intensity was increased (Fig. 4B). Examining measurements from a larger part of the dendrite revealed that [Ca$^{2+}$] transients were also present in some dendritic shafts (Fig. 4D). Transient bath application of the NMDAR antagonist AP5 (10 μM) reversibly abolished both the spine signals and those in the dendrites, indicating that they were mediated by synaptically activated NMDARs, possibly reflecting NMDA spikes (Schiller et al., 2000). These data show that the AOL microscope

can resolve spatially distributed synaptic activity in spines and dendrites using genetically encoded indicators.

### 3.3. Monitoring the timing of action potential backpropagation into a 3D dendritic tree

To test the temporal performance of the AOL microscope in detecting fast neuronal signalling in 3D, we examined the [$Ca^{2+}$] transients triggered by backpropagation of an AP into the dendritic tree. Fig. 5A shows a MIP and two individual $X$–$Y$ planes of a L2/3 pyramidal cell loaded with Alexa 594 and Fluo-4, revealing a dendritic tree that spanned ∼40 μm in depth. Fifteen POIs were defined along the main dendritic trunk and a secondary branch. Evoking a single AP at the soma, followed by a 10 Hz burst of 5 APs, triggered robust fast-rising low-noise [$Ca^{2+}$] transients at all locations (Fig. 5B; responses are single trials). To examine whether differences in the timing of the [$Ca^{2+}$] transients could be resolved at different locations, we averaged the transients across 10 trials and estimated their onset time by fitting the rising phase (Fig. 5C left). The relationship between onset time and distance of the POI from the soma revealed a significant correlation, despite some scatter in the onset times ($p$ = 0.00022; Fig. 5C right). Moreover, the slope of the linear fit was 0.17 m/s, a value similar to that estimated from dendritic patch-clamp recordings in L5 pyramidal cells (0.15 m/s) (Stuart and Sakmann, 1994) and recent measurements with a different AOL microscope design (0.23 m/s) (Katona et al., 2012). Analysis of the amplitude of the AP-evoked $\Delta F/R$ fluorescent transients showed that they varied considerably from location to location in the dendrite (Fig. 5D). This variation did not arise from depth-dependent changes in the SNR due to remote focusing (Fig. S2), and thus it seems that AP-evoked [$Ca^{2+}$] transients are heterogeneous, as previously suggested (Svoboda et al., 1999). These results illustrate how AOL microscopy can be used to track rapidly propagating neuronal signalling in 3D dendrites at a temporal resolution that has previously been the sole preserve of electrophysiology.

### 3.4. 3D functional imaging of neuronal population activity in vivo

To test the performance of the compact AOL microscope for *in vivo* measurements we performed functional imaging in primary visual cortex of anaesthetized mice. For this, we bolus loaded synthetic dyes (Stosiek et al., 2003) since they have been used extensively to study neuronal population activity.

#### 3.4.1. AOL depth penetration

To image signalling within neuronal populations *in vivo*, greater depth penetration is typically required than for acute slice preparations. Our structural imaging tests with OGB1-AM showed that the AOL microscope has sufficient laser power to Image 400 μm below the surface of the brain (Fig. S3).

#### 3.4.2. Monitoring the activity of 100 neurons distributed in 3D over 150 μm depth

Fig. 6A shows an example of a 3D field of view of a region of cortex loaded with green Fluo-4-AM, and the red neuronal tracer calcein-red orange-AM 180–330 μm below the pia. We selected 100 neurons distributed within this block of tissue and defined a single POI within the soma of each neuron (Fig. 6A–C). Simultaneous measurement from all 100 neurons at 360 Hz during visual presentation of drifting gratings with different orientations triggered [$Ca^{2+}$] transients in a subset of cells (Fig. 6D). Comparison of responses to different orientations in 2 consecutive sequences indicates that some neurons responded selectively to specific orientations (*e.g.*, cell 34), while others exhibited no detectable response to the stimulus (*e.g.*, cell 10). Responses of three neurons, located between 196 and 312 μm deep, to their preferred orientation are

shown on a faster timescale in Fig. 6E. Each cell exhibited a similar delay in the response when the same orientation was presented. However, a larger dispersion in the response latency was observed across cells responding to different orientations (Fig. 6E). These results show that the AOL microscope can be used *in vivo* to make high-speed functional measurements from populations of neurons distributed in 3D space. Importantly, tissue movement was minimal during *in vivo* recordings (Fig. S4) and the POI typically remained within the neuronal boundaries during recording (Fig. S5). However, experiments comparing the responses of two POIs placed within the same neuron suggest that, at some locations (*e.g.*, within the nucleus), the [$Ca^{2+}$] transient is too small to be detected reliably *in vivo* (Fig. S5). In the next section, we investigate the origin of this variability.

### 3.5. Temporal precision of action potential-evoked [$Ca^{2+}$] transients at points of interest in the perisomatic compartment in vitro

#### 3.5.1. Spatial dependence of [$Ca^{2+}$] transients in the perisomatic compartment in vitro

The amplitude and rise time of [$Ca^{2+}$] transients recorded *in vivo* from POIs in the same neuron exhibited a larger variability than those observed for AP-evoked responses in dendrites *in vitro* (Fig. S5 E and F, compare with Fig. 5B). To investigate the source of this variability, we made whole-cell patch-clamp recordings from L2/3 cells in slices and examined how the AP-evoked [$Ca^{2+}$] transient varied with location within the somato-dendritic compartment (Fig. 7A and B). The largest and fastest transients occurred in the dendrite and the smallest and slowest at the centre of the soma. We quantified the time course by fitting mean transient waveforms with exponentially rising and decaying functions (Fig. 7B), a procedure previously used to assess the temporal precision of action potential detection during calcium imaging with AODs (Grewe et al., 2010; Otsu et al., 2008). This showed that the peak $\Delta F/F$ was substantially higher in the dendrite compared to the centre of the soma, as previously shown (Svoboda et al., 1999). Moreover, the rise time varied from just 1.5 ms in the dendrite to 105 ms at the centre of the soma of this cell (Fig. 7C). This, together with a decay time course that was also much slower in the soma, made estimation of the onset time of the transients difficult. Analysis of single-trial [$Ca^{2+}$] transients using different temporal filters showed that somatic signals required heavier filtering than dendritic signals to achieve a comparable single-trial SNR (*i.e.*, 50 ms *vs* 5 ms; Fig. 7D and E). This limited the temporal precision with which the timing of the transients could be estimated at the soma. These results suggest that there is a 'sweet spot' that trades off the requirements of maximizing the size of the compartment from which the recording is made (making it robust to tissue movement) and minimizing the rise time of the transients. POIs at this sweet spot (Fig. 7F) gave transients with sufficiently good SNR to allow AP timing to be estimated within a <5 ms window with 95% confidence (Fig. 7G and H). On average, the 95% confidence interval was 2.8 ms ± 0.75 ms (range 1.5–4.7, $n$ = 4 experiments with 20–200 trials each, Mean ± SE). Moreover, individual transients could be distinguished during bursts of 25 Hz (Fig. 7I). Importantly, there was relatively little change in the properties of the transients or the electrophysiology during a 300 s acquisition, suggesting that detection from a single POI is reasonably robust to photodamage (Fig. S6). These results show that the spatial dependence of the kinetics and amplitude of AP-evoked [$Ca^{2+}$] transients in the somatic compartment recorded *in vitro* can account for much of the variability observed in sensory-evoked responses recorded *in vivo*.
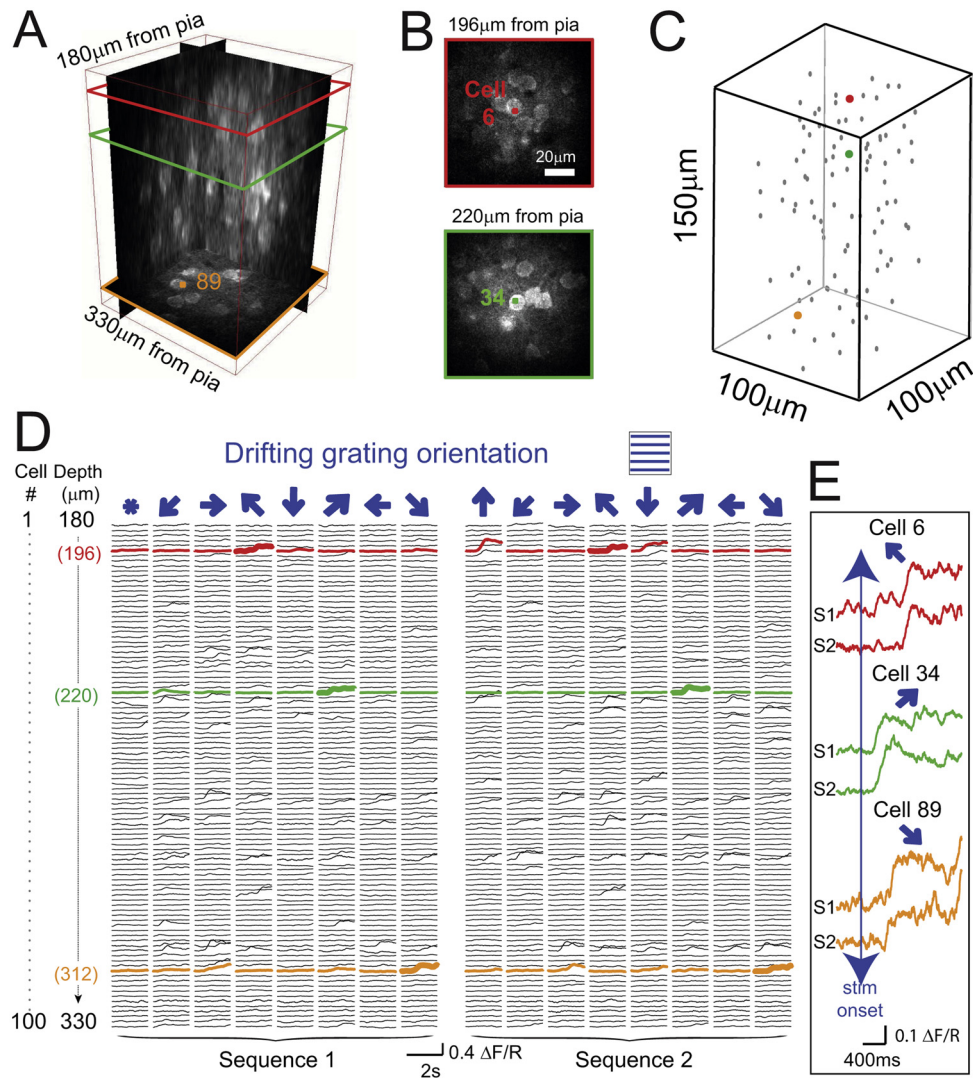
**Fig. 6.** *In vivo* AOL RAMP measurements from 100 neurons distributed in 3D within the primary visual cortex of an anaesthetized mouse.
(A) Structural image of a block of L 2/3 primary visual cortex (100 μm × 100 μm × 150 μm) bolus loaded with calcein-red orange-AM and the synthetic calcium indicator Fluo4-AM. The Z stack consisted of 38 planes spanning 180–330 μm from the pial surface. (B) Two *X–Y* planes at different depths colour coded as for A. (C) Schematic showing 100 POIs selected (one per neuron) for functional imaging within the tissue block. The location of POIs on 3 representative neurons (cells 6, 34 and 89) are shown in red, green and brown respectively, as illustrated in A and B. (D) Simultaneous [Ca²⁺] measurements from the 100 neurons distributed in 3D (180–330 μm depth; C) during presentation of drifting gratings of different orientations (arrows, vertical columns, drifting onset at 400 ms). Asterisk shows control with no visual stimulus presented. Left and right blocks show responses during two consecutive orientation sequences (traces filtered with 282 ms window). Coloured traces show examples of cells with orientation-tuned responses (as for A–C). (E) Single-trial recordings from cells 6, 34 and 89 (bold in D) filtered with a 56 ms window. Note trial-to-trial jitter in response onset for individual cell and onset difference between cells (stimulus onset time, blue arrow). Recording bandwidth was 36 kHz or 0.36 kHz/POI, including 4 μs dwell time. (For interpretation of the references to color in this figure legend, the reader is referred to the web version of this article.)

### 3.5.2. Comparison of signals at the centre of soma vs the 'sweet-spot'

Results from 7 experiments quantifying the transients in a somatic POI located in the junction with the dendrite showed that not only the Δ*F*/*F* and SNR was 2.5–3 times larger, but also the rise and decay times were > 10 times faster compared to a POI in the centre of the soma (Fig. 7E). This result suggest that future optimization in labelling techniques as well as 3D rendering where dendrites leaving the soma can be automatically identified during *in vivo* imaging can be exploited to significantly improve both detection and timing of AP-evoked calcium transients.

## 4. Discussion

We have tested the performance of a compact AOL microscope (Fig. 1) by measuring spatially distributed neuronal signalling in 3D *in vitro* and *in vivo*. Our results establish that the activity of many synaptic inputs distributed in 3D space can be monitored near simultaneously on a single trial with this new technology (Figs. 3 and 4). We confirm previous results (Katona et al., 2012) showing that the temporal resolution of AOL microscopy is sufficient to track the backpropagation of an AP into a 3D dendrite with sub-millisecond temporal precision (Fig. 5) and that 3D neuronal population activity patterns can be measured *in vivo* as they respond to sensory input (Fig. 6 and S5). Here we have combined, for the first time, AOL-based 3D imaging with genetically encoded indicators (Fig. 4 and Fig. S1) and explored strategies for optimizing functional imaging of neuronal populations (Fig. 7). Our results establish that AOL microscopy has the performance and flexibility to monitor rapid neuronal signalling in 3D across a wide range of spatial scales using both synthetic and genetically encoded reporters.
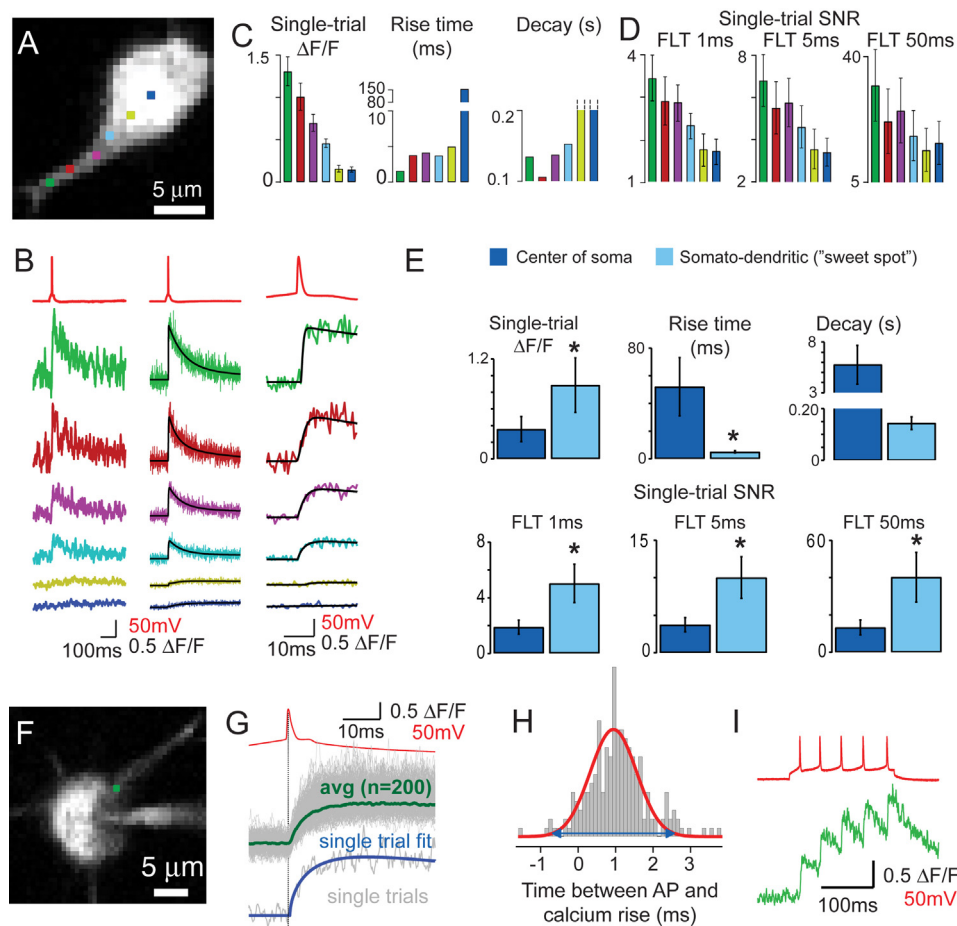
**Fig. 7.** Spatial heterogeneity of [Ca²⁺] transients in somato-dendritic compartment and estimation of action potential timing.

(A) Structural image of a cortical L2/3 cell patch loaded with Alexa 594 and Fluo-4. Coloured pixels indicate POIs along the soma and proximal dendrite. (B) AP-evoked [Ca²⁺] transients ($\Delta F/F$) in POIs shown in A (same colour codes). A single trial (filtered with 5 ms window, left), and the average of 20 unfiltered trials (fits in black) is shown in the middle and with enlarged temporal scale in the right (1.9 kHz acquisition rate). (C) Comparison of single-trial $\Delta F/F$ (Mean +/−SD for 20 trials) and 10–90% rise time and decay time at the different POIs shown in A. (D) SNR [Ca²⁺] transients following processing with different length boxcar filter (FLT) windows. (E) Pool data from 7 experiments. Comparison of AP-evoked [Ca²⁺] transients in a POI at the centre of the soma (dark blue) *vs* a POI at the junction with the proximal dendrite (light blue). * indicates a significant difference between the population means ($p < 0.05$, Wilcoxon Signed test). Error bars are standard error of the mean. (F) POI location (green pixel) on L2/3 cell with reasonable trade-off between compartment size and SNR. (G) AP-evoked [Ca²⁺] transients for 200 trials acquired at 5.8 kHz (filtered with 1 ms window). Whole-cell voltage recording in red, individual [Ca²⁺] transients in grey, average in green. Below: individual transient (grey) fit with a tri-exponential function (blue trace). (H) Histogram of interval between the peak of the measured AP and the time at which the fitted function rose to 10% of its peak value. A Gaussian fit (red) to the interval histogram indicates that the estimated AP time was distributed normally, and the 95% confidence could be determined from 4 × S.D. (blue arrow). (I) Single-trial AP-evoked [Ca²⁺] transients (data filtered with 1 ms window) in response to a burst of 5 APs at ~25 Hz. (For interpretation of the references to color in this figure legend, the reader is referred to the web version of this article.)

## 4.1. Design features of the acousto-optic lens 3D 2-photon microscope

A number of the design features of our AOL microscope (Kirkby et al., 2010) and its functionality differ from other AOL 3D microscopes (Duemani Reddy et al., 2008; Katona et al., 2012). The thin optically and acoustically rotated AOD crystals allow a simple and compact AOL design that can operate over a range of different excitation wavelengths, with relatively little chromatic (see also (Duemani Reddy et al., 2008)) or temporal dispersion. This allows the device to be easily added to an existing 2-photon microscope, enabling rapid remote focusing and scanning of a femtosecond laser beam, with the only additional modification of a more powerful prism-based prechirper (Kirkby et al., 2010). These features have allowed us to perform low-power, high-temporal resolution imaging of spines. Moreover, the ability to change excitation wavelength without moving the optical elements within the AOL has allowed us to combine 3D AOL two-photon microscopy with genetically

encoded [Ca²⁺] indicators (Fig. 4 and Fig. S1), which operate at longer excitation wavelengths than green synthetic dyes (Fig. 3). As we show, this enables measurement from specific neuronal sub-types (*e.g.*, L2/3 pyramidal cells).

## 4.2. Utility of compact AOL-based 3D random access measurements for functional imaging

The fact that electrical signalling events in the brain are brief (1–100 ms) and sparsely distributed in 3D space makes them particularly difficult to monitor with conventional two-photon laser scanning microscopy. Unlike scanning systems with mirrors that have inertia (Botcherby et al., 2012; Gobel et al., 2007), our AOL 3D microscope has a high bandwidth (36 kHz) and a voxel access time that is independent of distance, making it particularly well suited for measuring rapid, sparsely distributed signals in 3D (Fig. 1C). The high spatial resolution of our AOL allowed us to resolve spines over a 150 μm focal range (Fig. 2), while our proof-of-principle

experiments show that AOL-based microscopy can be used for functional [Ca$^{2+}$] measurement in spines and dendritic shafts. We establish that it is now possible to simultaneously monitor the activity of synaptic inputs at many different locations on the 3D dendritic tree of pyramidal neurons (Figs. 3–5). We also confirm (Katona et al., 2012) that our AOL microscope design has sufficient temporal resolution to determine the speed of AP backpropagation from the timing of AP-evoked [Ca$^{2+}$] transients at multiple locations along a 3D dendritic tree (Fig. 5). AOL-based 3D microscopy therefore has the spatial resolution and speed necessary for measuring the spatio-temporal patterns of synaptic input onto a dendritic tree. This will be particularly useful for studies of spike timing dependent plasticity (Sjostrom et al., 2008), and for understanding the computations that individual neurons perform (Silver, 2010), as well as the underlying mechanisms (Bloodgood and Sabatini, 2007; Chalifoux and Carter, 2011; Noguchi et al., 2005). Moreover, this technology is likely to be to useful for mapping the receptive field of synaptic inputs onto dendritic arborisations, which have been limited to the simultaneous read-out of a few spines located in the same focal plane (Chen et al., 2011). This will make it easier to test hypotheses regarding the spatio-temporal clustering of synaptic input on the dendritic tree during sensory input (Larkum and Nevian, 2008).

We have established that it is possible to operate our AOL at the longer wavelengths necessary to excite genetically encoded indicators. The ability to combine AOL 3D microscopy with genetically encoded reporters is an important development because, unlike synthetic dyes, they can be expressed selectively in specific neuronal subpopulations. High speed imaging will allow the investigation of the types of sensory information being conveyed by axons and enable synaptic inputs to be studied over extended periods of time, revealing how their functional properties change with experience and during development (Mank et al., 2008).

We have also shown that our AOL can deliver sufficient laser power for measuring neural population activity deep within a 3D block of cortex *in vivo*, confirming previous results (Katona et al., 2012). The experiments were carried out with a fully back filled 40 × 0.8 NA objective to attain a high spatial resolution. This resulted in a smaller field of view than that previously reported (Katona et al., 2012). However, the field of view of our system can be substantially increased by using a 20× objective and a lower numerical aperture (Fig. S1 A and B, Supplementary Table 1), an approach that is well suited to imaging the activity of a larger population of neurons (Grewe et al., 2010; Katona et al., 2012). During presentation of a visual stimulus, the activity of 100 neurons distributed over ~150 μm in depth was monitored simultaneously at high rates and latency information obtained (Fig. 6). This opens the possibility of using optical imaging to investigate the extent to which the brain uses temporal sequences to encode and process information (Gollisch and Meister, 2008; Johansson and Birznieks, 2004). In addition, the depth penetration and focusing range of the AOL will potentially enable the study of the flow of information across layers located at different focal depths (*e.g.*, L4 and L2/3). Moreover, the ability to monitor from sparsely distributed points in 3D and genetically labelled neurons will also facilitate the study of low density neuronal subtypes (*e.g.*, interneurons), which are currently difficult to study with 2D microscopy.

Our results show that *in vivo* 3D-RAMP recordings require further optimization if we are to attain the < 5 ms precision in estimating AP timing that we can achieve *in vitro*. This is due to the large spatial heterogeneity in the responses in the somato-dendritic compartment. Improvements in SNR can be achieved with spatial averaging: either by increasing the size of the illumination point-spread function (with a lower NA) and/or by making multiple point measurements from each somata. Both of these strategies have been used for 2D RAMP imaging *in vivo*, enabling the timing of APs to be estimated from [Ca$^{2+}$] transients with a temporal precision

of ~10 ms (Grewe et al., 2010). The disadvantage of increasing the number of recording locations per cell is that it reduces the acquisition rate. Alternatively, we found that the junction between the soma and primary dendrite provides a 'sweet spot' where the amplitude and speed of transients is higher than the centre of the soma. Making point measurements from this region has a higher SNR and has the advantage that it does not compromise the speed of acquisition (Fig. 7).

### 4.3. Future prospects and challenges

The unprecedented temporal resolution of AOL-based 3D functional imaging together with the advances shown here, demonstrate that it is a flexible tool for addressing a range of questions in cellular and systems neuroscience. The feasibility of measuring the spatiotemporal patterns of synaptic input onto a 3D dendrite, the ability to simultaneously monitor the activity of a large number of dendrites on a neuron and the capacity to readout the sequence of activation of a neuronal population distributed in 3D space should be useful for studying how the brain rapidly represents and transforms information at synaptic, neuronal and network levels. Our demonstration of the feasibility of combining AOL microscopy with genetic indicators opens the possibility of high speed 3D measurements from a range of identified neurons (Hofer et al., 2011), as well as chronic functional imaging studies (Mank et al., 2008) which are difficult with synthetic dyes. However, application of 3D RAMP to the awake head-fixed animal preparation (Dombeck et al., 2010; Petreanu et al., 2012) will require the development of rapid online movement correction, particularly for monitoring signalling in small structures. While at present the power throughput may not be sufficient to photoactive MNI-glutamate (Fig. 1A, inset), compounds with higher two-photon cross sections, and/or improvements in AOL design or more powerful lasers should make rapid 3D neural activation feasible. The high bandwidth of the AOL combined with the continued improvement in the SNR of voltage-sensitive dyes (Akemann et al., 2012; Bradley et al., 2009; Zhou et al., 2007) make optical measurement of voltage across 3D dendritic trees, axons and local networks feasible in the near future. Another exciting short-term prospect is to combine the long wavelength excitation AOL microscopy described here with a recently developed genetically encoded glutamate sensor (Marvin et al., 2013), since this will enable synaptic glutamate release to be mapped at high spatio-temporal resolution onto the 3D dendrites of genetically distinct neuronal populations.

## 5. Conclusion

We have demonstrated new applications of AOD-based rapid functional imaging in 3D using a custom-designed acousto-optic lens (AOL) which has a compact design and can be introduced in existing two-photon microscopes. We showed that our AOL can be operated at a range of wavelengths and have exploited this flexibility to establish that genetically encoded indicators can be used with this technology. We also showed that dendritic spines can be resolved over 150 μm depth range within the AOL volumetric field of view and demonstrated the utility of AOL two-photon microscopy to read-out, simultaneously, 3D patterns of synaptic activity.

### Conflict of interest

Patents on the AOL technology have been filed (WO/2008/032061, WO/2011/131933, WO/2012/143702).

## Author contributions

TFA and RAS planned the experiments and wrote the manuscript. TFA performed the *in vitro* experiments. KMNSN developed the control and acquisition software. MFI and TFA performed the *in vivo* experiments. TFA analyzed the data. BP contributed to the initial software design and code. HR performed the *in utero* electroporation. PK, KMNSN and RAS developed the AOLM. RAS supervised the project.

## Acknowledgements

## Appendix A. Supplementary data

Supplementary material related to this article can be found, in the online version, at http://dx.doi.org/10.1016/j.jneumeth.2013.10.021.

## References

Agmon A, Connors BW. Thalamocortical responses of mouse somatosensory (barrel) cortex in vitro. Neuroscience 1991;41:365–79.

Akemann W, Mutoh H, Perron A, Park YK, Iwamoto Y, Knopfel T. Imaging neural circuit dynamics with a voltage-sensitive fluorescent protein. J Neurophysiol 2012;108:2323–37.

Bloodgood BL, Sabatini BL. Ca(2+) signaling in dendritic spines. Curr Opin Neurobiol 2007;17:345–51.

Bollmann JH, Engert F. Subcellular topography of visually driven dendritic activity in the vertebrate visual system. Neuron 2009;61:895–905.

Bonifazi P, Goldin M, Picardo MA, Jorquera I, Cattani A, Bianconi G, et al. GABAergic hub neurons orchestrate synchrony in developing hippocampal networks. Science 2009;326:1419–24.

Botcherby EJ, Smith CW, Kohl MM, Debarre D, Booth MJ, Juskaitis R, et al. Aberration-free three-dimensional multiphoton imaging of neuronal activity at kHz rates. Proc Natl Acad Sci U S A 2012;109:2919–24.

Bradley J, Luo R, Otis TS, DiGregorio DA. Submillisecond optical reporting of membrane potential in situ using a neuronal tracer dye. J Neurosci 2009;29:9197–209.

Brainard DH. The psychophysics toolbox. Spat Vis 1997;10:433–6.

Chaigneau E, Wright AJ, Poland SP, Girkin JM, Silver RA. Impact of wavefront distortion and scattering on 2-photon microscopy in mammalian brain tissue. Opt Express 2011;19:22755–74.

Chalifoux JR, Carter AG. Glutamate spillover promotes the generation of NMDA spikes. J Neurosci 2011;31:16435–46.

Chen X, Leischner U, Rochefort NL, Nelken I, Konnerth A. Functional mapping of single spines in cortical neurons in vivo. Nature 2011;475:501–5.

Denk W, Strickler JH, Webb WW. Two-photon laser scanning fluorescence microscopy. Science 1990;248:73–6.

Dombeck DA, Harvey CD, Tian L, Looger LL, Tank DW. Functional imaging of hippocampal place cells at cellular resolution during virtual navigation. Nat Neurosci 2010;13:1433–40.

Duemani Reddy G, Kelleher K, Fink R, Saggau P. Three-dimensional random access multiphoton microscopy for functional imaging of neuronal activity. Nat Neurosci 2008;11:713–20.

Gobel W, Kampa BM, Helmchen F. Imaging cellular network dynamics in three dimensions using fast 3D laser scanning. Nat Methods 2007;4:73–9.

Gollisch T, Meister M. Rapid neural coding in the retina with relative spike latencies. Science 2008;319:1108–11.

Grewe BF, Langer D, Kasper H, Kampa BM, Helmchen F. High-speed in vivo calcium imaging reveals neuronal network activity with near-millisecond precision. Nat Methods 2010;7:399–405.

Harvey MA, Saal HP, Dammann JF 3rd, Bensmaia SJ. Multiplexing stimulus information through rate and temporal codes in primate somatosensory cortex. PLoS Biol 2013;11:e1001558.

Helmchen F, Denk W. Deep tissue two-photon microscopy. Nat Methods 2005;2:932–40.

Higley MJ, Sabatini BL. Calcium signaling in dendritic spines. Cold Spring Harb Perspect Biol 2012;4:a005686.

Hofer SB, Ko H, Pichler B, Vogelstein J, Ros H, Zeng H, et al. Differential connectivity and response dynamics of excitatory and inhibitory neurons in visual cortex. Nat Neurosci 2011;14:1045–52.

Jia H, Rochefort NL, Chen X, Konnerth A. Dendritic organization of sensory input to cortical neurons in vivo. Nature 2010;464:1307–12.

Johansson RS, Birznieks I. First spikes in ensembles of human tactile afferents code complex spatial fingertip events. Nat Neurosci 2004;7:170–7.

Junek S, Kludt E, Wolf F, Schild D. Olfactory coding with patterns of response latencies. Neuron 2010;67:872–84.

Kaplan A, Friedman N, Davidson N. Acousto-optic lens with very fast focus scanning. Opt Lett 2001;26:1078–80.

Katona G, Kaszas A, Turi GF, Hajos N, Tamas G, Vizi ES, et al. Roller coaster scanning reveals spontaneous triggering of dendritic spikes in CA1 interneurons. Proc Natl Acad Sci U S A 2011;108:2148–53.

Katona G, Szalay G, Maak P, Kaszas A, Veress M, Hillier D, et al. Fast two-photon in vivo imaging with three-dimensional random-access scanning in large tissue volumes. Nat Methods 2012;9:201–8.

Kerr JN, de Kock CP, Greenberg DS, Bruno RM, Sakmann B, Helmchen F. Spatial organization of neuronal population responses in layer 2/3 of rat barrel cortex. J Neurosci 2007;27:13316–28.

Kerr JN, Greenberg D, Helmchen F. Imaging input and output of neocortical networks in vivo. Proc Natl Acad Sci U S A 2005;102:14063–8.

Kirkby PA, Srinivas Nadella KM, Silver RA. A compact acousto-optic lens for 2D and 3D femtosecond based 2-photon microscopy. Opt Express 2010;18: 13721–45.

Ko H, Hofer SB, Pichler B, Buchanan KA, Sjostrom PJ, Mrsic-Flogel TD. Functional specificity of local synaptic connections in neocortical networks. Nature 2011;473:87–91.

Larkum ME, Nevian T. Synaptic clustering by dendritic signalling mechanisms. Curr Opin Neurobiol 2008;18:321–31.

Mank M, Santos AF, Direnberger S, Mrsic-Flogel TD, Hofer SB, Stein V, et al. A genetically encoded calcium indicator for chronic in vivo two-photon imaging. Nat Methods 2008;5:805–11.

Marvin JS, Borghuis BG, Tian L, Cichon J, Harnett MT, Akerboom J, et al. An optimized fluorescent probe for visualizing glutamate neurotransmission. Nat Methods 2013;10:162–70.

Nielsen TA, DiGregorio DA, Silver RA. Modulation of glutamate mobility reveals the mechanism underlying slow-rising AMPAR EPSCs and the diffusion coefficient in the synaptic cleft. Neuron 2004;42:757–71.

Nikolenko V, Watson BO, Araya R, Woodruff A, Peterka DS, Yuste R. SLM microscopy scanless two-photon imaging and photostimulation with spatial light modulators. Front Neural Circuits 2008;2:5.

Noguchi J, Matsuzaki M, Ellis-Davies GC, Kasai H. Spine-neck geometry determines NMDA receptor-dependent $Ca^{2+}$ signaling in dendrites. Neuron 2005;46:609–22.

Ohki K, Chung S, Ch'ng YH, Kara P, Reid RC. Functional imaging with cellular resolution reveals precise micro-architecture in visual cortex. Nature 2005;433:597–603.

Otsu Y, Bormuth V, Wong J, Mathieu B, Dugue GP, Feltz A, et al. Optical monitoring of neuronal activity at high frame rate with a digital random-access multiphoton (RAMP) microscope. J Neurosci Methods 2008;173: 259–70.

Pelli DG. The videotoolbox software for visual psychophysics: transforming numbers into movies. Spat Vis 1997;10:437–42.

Petreanu L, Gutnisky DA, Huber D, Xu NL, O'Connor DH, Tian L, et al. Activity in motor-sensory projections reveals distributed coding in somatosensation. Nature 2012;489:299–303.

Rothschild G, Nelken I, Mizrahi A. Functional organization and population dynamics in the mouse primary auditory cortex. Nat Neurosci 2010;13: 353–60.

Saito T, Nakatsuji N. Efficient gene transfer into the embryonic mouse brain using in vivo electroporation. Dev Biol 2001;240:237–46.

Salome R, Kremer Y, Dieudonne S, Leger JF, Krichevsky O, Wyart C, et al. Ultra-fast random-access scanning in two-photon microscopy using acousto-optic deflectors. J Neurosci Methods 2006;154:161–74.

Sato TR, Gray NW, Mainen ZF, Svoboda K. The functional microarchitecture of the mouse barrel cortex. PLoS Biol 2007;5:e189.

Schiller J, Major G, Koester HJ, Schiller Y. NMDA spikes in basal dendrites of cortical pyramidal neurons. Nature 2000;404:285–9.

Silver RA. Neuronal arithmetic. Nat Rev Neurosci 2010;11:474–89.

Sjostrom PJ, Rancz EA, Roth A, Hausser M. Dendritic excitability and synaptic plasticity. Physiol Rev 2008;88:769–840.

Stosiek C, Garaschuk O, Holthoff K, Konnerth A. In vivo two-photon calcium imaging of neuronal networks. Proc Natl Acad Sci U S A 2003;100:7319–24.

Stuart GJ, Sakmann B. Active propagation of somatic action potentials into neocortical pyramidal cell dendrites. Nature 1994;367:69–72.

Svoboda K, Helmchen F, Denk W, Tank DW. Spread of dendritic excitation in layer 2/3 pyramidal neurons in rat barrel cortex in vivo. Nat Neurosci 1999;2: 65–73.

Tabata H, Nakajima K. Efficient in utero gene transfer system to the developing mouse brain using electroporation: visualization of neuronal migration in the developing cortex. Neuroscience 2001;103:865–72.

Tian L, Hires SA, Mao T, Huber D, Chiappe ME, Chalasani SH, et al. Imaging neural activity in worms, flies and mice with improved GCaMP calcium indicators. Nat Methods 2009;6:875–81.

Vucinic D, Sejnowski TJ. A compact multiphoton 3D imaging system for recording fast neuronal activity. PLoS ONE 2007;2:e699.

Zhou WL, Yan P, Wuskell JP, Loew LM, Antic SD. Intracellular long-wavelength voltage-sensitive dyes for studying the dynamics of action potentials in axons and thin dendrites. J Neurosci Methods 2007;164:225–39.

Zipfel WR, Williams RM, Webb WW. Nonlinear magic: multiphoton microscopy in the biosciences. Nat Biotechnol 2003;21:1369–77.